# Final Technical Report - NAG 5 532 - "Flexural Deformation of the Continental Lithosphere"

p. 23

The following is the final report for NASA grant NAG 5 532 awarded to Leigh Royden for study of flexure of the continental lithosphere. Despite the fact that this is the final report for this grant, work on this topic is expected to continue under another award from NASA. Thus not all of our studies are complete and work is continuing on many of these topics.

Work accomplished prior to 1990 focused primarily on the Adriatic and northern Ionian regions. The results of these studies have been summarized in a previous proposal submitted to NASA, and so are only briefly summarized below. More recent work focuses on two different topics: (1) analysis of foredeep basin geometry, sedimentary style, and thrust belt structure in light of the kinematics at the associated plate boundary and subduction zone dynamics, and (2) the evolution and plate strength of early Proterozoic lithosphere. These newer results, obtained in 1990 and spring, 1991, are described in more detail. In all, four published papers and one PhD thesis have resulted from this project since 1987. Two additional manuscrips are nearing completion.

## I) The Adriatic-Ionian Region:

### Method

A method for simultaneous fitting of gravity and basin depth data to determine the flexural behavior of foreland lithosphere has been developed and refined throughout the study period. This technique enables one to fit gravity and deflection data along any profile, and to determine the effective elastic strength of the deflected lithosphere (in so far as the data constrain a unique solution), the initial water depth, and the vertical load (in addition to the topographic load) and bending moment that act on the deflected lithosphere. Prior to 1990 we primarily used this method to examine the flexural development of the Adriatic foredeep basin.

### Pliocene Plate Flexure of the Apennine Foreland

Examination of several transects across the Apennine mountains and Adriatic foredeep basin has shown good to excellent agreement between observed gravity and Pliocene to Recent deflection and gravity and deflection predicted by a simple elastic plate model with effective elastic plate thickness between 10 and 20 km (depending on the profile analyzed). All of these profiles require

in modern foreland basins. We do not know if the strength of the Slave craton at 1.9 Gyr is representative of the strength for early Proterozoic continental lithosphere in general. If it is a particularly weak example of early Proterozoic lithosphere then the average strength of early Proterozoic lithosphere need not have been significantly different from that today. On the other hand, we cannot rule out the possibility that the Slave craton is a particularly strong example of early Proterozoic lithosphere, in which case the average elastic plate thickness of early Proterozoic lithosphere may have been as much as an order of magnitude less than that today, implying that geothermal gradients may have been a factor of 2-3 times greater than today. Unfortunately, the great range of flexural rigidities observed for foreland basins today and the lack of a representative sampling of ancient rigidities make it impossible to be more definitive.

This work is published in Grotzinger and Royden (1990).

## III) Systematic Correlation of Foredeep Basin Geometry and Facies with Tectonic Setting (in Light of Subduction Zone Dynamics):

Within the broad spectrum of foredeep basin types that are developed on continental lithosphere, it is possible to identify different end-member types, both in terms of the basin geometry and its relationship to the size of the adjacent thrust belt, and in terms of the large-scale sedimentary facies that comprise the basin fill. The thrust belts adjacent to these basins likewise display display distinctly different structural styles and correspond to two different end-members within a broad spectrum of thrust belt types. Over the last year we have examined systematic correlations between basin geometry, sedimentary facies and thrust belt style by examining obvious end-member examples. In a greatly simplified and generalized form these end-member types can be summarized as follows:

Basin Geometry:

On one end of the spectrum are basins whose depth and flexural shape appear to be largely the result of loading of the foreland lithosphere by advancing thrust sheets and are consistent with the size of the mountain belt adjacent to the basin. If large subsurface loads act on the subducted plate in these systems, they must be applied at sufficient distance from the basin that they do not contribute significantly to the flexure of the lithosphere immediately under the basin. On the other end of the spectrum are basins whose depth and flexural shape appear to be largely the result of subsurface (subduction) loads acting on the subducted plate at depth. The topographic load represented by the size of the adjacent mountain belt contributes only negligibly to the flexure of the lithosphere beneath the basin. Between these two end-member examples are a wide range of foredeep basins whose

flexural shape is due in part to the topographic load represented by the adjacent mountain belt and in part to subsurface loads acting on the subducted slab at depth.

Large Scale Sedimentary Facies:

A cursory examination of the large scale facies patterns present in foreland basins suggests that two basic end-member types exist: "molasse" basins within which predominantly coarse clastic sediments (sandstone, conglomerates, etc.) are deposited in primarily non-marine to shallow marine conditions, and "flysch" basins within which predominantly fine grained clastic sediments (silts, shales, turbidites, etc.) are deposited in primarily shallow to deep marine conditions.

Thrust Belt Style:

Continental subduction zones and orogenic belts also exhibit two distinct structural styles that represent end-member types within a broad range of possible structural styles. On one end of the spectrum are belts that exhibit no regional back-arc extension adjacent to the thrust belt. These belts are commonly typified by extensive involvement of crystalline basement in thrusting, exposure of high grade metamorphic rocks at the surface, high topographic elevation, and large amounts of denudation (tens of kilometers). On the other end of the spectrum are belts that exhibit back-arc extension contemporaneously with thrusting. These belts are commonly typified by little to no involvement of crystalline basement in thrusting, low grade to no metamorphism, low topographic elevation and little denudation.

In order to test for systematic correlations exist between end-member examples of basin geometry, large-scale sedimentary facies, and thrust belt style, we selected five young to active thrust belts and their associated foredeep basins: the Himalayas, the Western to Eastern (and Southern) Alps, the Apennines, the Carpathians, and the Hellenides (Figure 3). Of these five thrust belts, the Himalayas and the Alps appear to be typical examples of thrust belts that form by shortening and convergence without development of regional extensional structures. They both comprise topographically large mountains with exposure of high grade metamorphic rocks at the surface. Crystalline rocks of the downgoing plate are extensively involved in the deformation and tens of kilometers of denudation has occurred within both mountain belts. The foredeep basins adjacent to the thrust belts contain predominantly of molassic facies deposited during a protracted history of post-collisional convergence. (Extensive references are available to document the structural style of all five belts, and are included in manuscript in preparation. however, we have been omitted from this proposal.)

The remaining three belts, the Apennines, the Carpathians and the Hellenides, appear to be typical examples of thrust belts that form adjacent to a zone of regional back-arc extension that is coeval with subduction and thrusting. All comprise topographically low mountains without exposure of medium to high grade metamorphic rocks at the surface. In general the crystalline basement of the downgoing plate has not been involved in deformation and is not exposed at shallow structural levels. Large amounts of erosion are lacking. The foredeep basins adjacent to the thrust belts contain predominantly flysch-like facies, and the thrust sheets in the outer parts of the belts are also composed largely of flysch that was probably deposited in older foredeep basins that have now been incorporated into the thrust belts. These convergent systems have thus experienced a protracted history of flysch deposition that has not been replaced by a transition to molassic sedimentation even in those areas where convergence and thrusting are now inactive.

Flexural analysis of six profiles through these five belts were analyzed using gravity and basin depth data. The results for two of these basins, the Apennine and Himalayan foredeep basins, are summarized in Figures 4 and 5. For both basins a good fit between the observed and computed basin depths and Bouguer gravity anomalies was obtained, provided that appropriate vertical shear forces and bending moments were applied to the effective plate end beneath the adjacent mountain belts. Because analysis of gravity data indicates that the vertical shear force required to act on the plate end cannot be due to a dense mass present at depths less than about 50 km, this end load is presumed to be due to forces acting on the subducted plate at depth, including the negative buoyancy of the subducted slab (see Royden, 1988, for a more detailed discussion). Figures 4 and 5 also show the result of applying only these end-loads and end-moments to the effective elastic plate end and neglecting the effects of topographic loading due to the adjacent mountains (see Figure 6 for cartoon of topographic and end loads).

It is clear that there is a dramatic difference in the source of the loads that cause the subsidence of the Himalayan and the Apennine foredeep basins. In the case of the Himalayas, the end-loads and end-moments acting on the overthrust plate contribute almost nothing to the plate flexure. The basin shape is due almost entirely to loading of the down-going plate by thrust sheets, and the geometry of the basin corresponds well to the size and shape of the adjacent mountain belt. In the case of the Apennines, the end-loads and end-moments acting on the overthrust plate cause almost all of the basin subsidence. Only a very small fraction of the subsidence can be explained by loading by thrust sheets and by the size and shape of the adjacent mountain belt. Thus these two basins, which represent end-member types in terms of sedimentary facies and in terms of the structural style of the associated thrust belt, also represent end-member

types in terms of the driving mechanism for flexural subsidence of the foreland lithosphere beneath the basin. Analysis of profiles across the three other thrust belts listed above yield similar results.

These results can perhaps be best understood in light of the size of the topographic load acting on the foreland lithosphere (eg the size of the mountains) and the position at which that load is applied. Figure 7 shows two idealized situations both involving subducted plates subjected to the same end-loads ($2 \cdot 10^{12}$ N/m) and end-moments ($10^{13}$ N). In the first case the thrust belt is thrust only a short distance beyond the effective plate end and corresponds to mountains with an average elevation of only 1 km (the Apennine analog). In the second case the thrust belt is thrust a great distance beyond the effective plate end and corresponds to mountains with an average elevation of 5 km (the Himalayan analog). When the total deflection of the foreland lithosphere is separated into the two components, in the first case (Apennine analog) the mountains contribute little to the basin subsidence and most of the subsidence is due to the end-loads. In the second case (Himalayan analog) the end-loads contribute the same amount to the flexure of the foreland lithosphere as in the first case, but the lateral position at which this flexure occurs is located far under the mountain belt. It has no effect on the flexure in front of the mountain belt only because it is applied too far from the mountain front. Thus the only source of load that contributes significantly to the subsidence in front of the mountains is the topographic load represented by the mountain belt itself.

Thus the differences in basin geometry relative to the size of the adjacent mountains can be best understood by the extent to which the foreland lithosphere has been overthrust by the thrust belt. In the case of the Himalayan end-member, the thrust-belt has been thrust out over parts of the foreland that are a long way from the subduction zone and that show no flexural subsidence as a result of loads applied to the subducted plate. In the case of the Apennine end-member, the thrust belt sits much closer to the subduction zone and the foreland lithosphere in front of the mountains has been greatly deflected by loads applied to the subducted plate. This suggests that the primary factor controlling this phenomena may be the magnitude of horizontal compressional stress transmitted across the convergent zone, relatively large horizontal compressional stresses acting to push the thrust sheets over the foreland in the Himalayan example, and relatively small horizontal compressional stresses acting on the thrust sheets in the Apennine example.

This interpretation is consistent with the major structural features within the two different thrust belts, especially with the presence (Apennines) or absence (Himalayas) of regional back-arc extension coeval with subduction and thrusting. The presence of back-arc extension behind an active subduction zone indicates that the rate of subduction of the foreland exceeds the rate of

overall plate convergence, implying poor mechanical coupling between the over-riding and down-going plates and thus little transmission of horizontal compressional stresses (above lithostatic). The absence of back-arc extension behind an active subduction zone indicates that the rate of subduction of the foreland is equal to or slower than the rate of subduction, implying strong mechanical coupling between the over-riding and down-going plates and thus allows transmission of large compressional stresses. Other workers have come to a similar conclusion for oceanic subduction systems, and pointed out that this is in accord with observations that very large subduction-related earthquakes occur only in those systems where back-arc extension is lacking, hence with good mechanical coupling between the two plates. The presence or absence of large horizontal compressional stresses is also consistent with the other structural differences between the two types of thrust belt. Thus it is possible to understand differences in structural style and foredeep basin geometry as the result of the level of mechanical coupling between over-riding and down-going plates, and the magnitude of the horizontal compressional stress transmitted across the subduction boundary.

How does this affect the sedimentary facies present in the foreland basins? In the Himalayan analogs, the basin forms only because of loading of the underlying lithosphere by the adjacent mountains. It is not possible to develop a deep basin without the presence of topographically high mountains adjacent to the basin, and in addition the mountains in these types of systems tend to be very high (Figure 8). Thus a major sediment source is always present next to the basin and large topographic gradients are present to provide transport for very coarse sediments into the basin. These basins tend to remain filled to sea level or above, to contain a large fraction of coarse clastic material, and to receive much of their sedimentary fill by down-slope transport perpendicular to the strike of the basin. This is almost the definition of a molasse-filled basin.

In the Apennine analogs, the basins form because of loads acting on the down-going plate from within the subduction zone. Topographically high mountains are generally lacking and the small mountains that do form commonly sit a great distance from the foredeep basin. Thus very deep basins can form without a great sediment source being present adjacent to the basin, and large topographic gradients perpendicular to the strike of the basin are commonly absent. Sedimentation in these basins often occurs in relatively deep water forming long linear regions of deep water down the axis of the basin. Sediments are largely transported down the axis of the basin, and with little topographic slope available to enable transport of coarse clastic material, the basin fill consists predominantly of fine-grained material. This is almost the definition of a flysch-filled basin.

The preceeding discussion indicates that there is a natural link between structural styles present in thrust belts, the flexural geometries of the adjacent foredeep basins and the large scale sedimentary facies that fill the basins. The controlling factor appears to be the degree of mechanical coupling between the over-riding and the down-going plates, and therefore the magnitude of the horizontal compressional stress transmitted across the subduction boundary. This is an exciting result because it ties together processes occurring within the mantle (subduction processes and driving forces, and relative plate velocities), processes occurring within the crust (development of structure within thrust-belts, and back-arc crustal extension), and surficial processes (sediment type, provenance, and mode of transport) within a single coherent framework. To my knowledge this is the first time that this has been done for convergent systems in such a comprehensive fashion, and even the basic concept is completely new.

## PUBLICATIONS TO DATE

Four papers resulting from this study have been published to date. A fifth in nearing completion (Royden), with a sixth anticipated for completion by June, 1991 (S. Kruse). A seventh manuscript on the Ionian region exists in very preliminary form (D. Dinter).

Publications to date:

Royden, L., E. Patacca and P. Scandone, 1987, Segmentation and configuration of subducted lithosphere in Italy: an important control on thrust belt and foredeep basin evolution, Geology, v. 15, p. 714-717.

Royden, L., 1988, Flexural behavior of the continental lithosphere in Italy: Constraints imposed by gravity and deflection data, J. Geophys. Res., v. 93, p. 7747-7766.

Moretti, I. and L. Royden, 1988, Deflection, gravity anomalies and tectonics of doubly subducted continental lithosphere: Adriatic and Ionian Seas: Tectonics, v. 7, p. 875-893.

Grotzinger, J. and L. Royden, 1990, Elastic strength of the Slave craton at 1.9 Gyr and implications for the thermal evolution of the continents, Nature, v. 347, no. 6288, p. 64-66.

Manuscripts to be submitted (shortly):

Royden, L., Systematic correlation of foredeep basin geometry ;and facies with tectonic setting.

Kruse, S. and L. Royden, Flexure of the Adriatic lithosphere (Italy) from Eocene to Recent time.

Preliminary manuscripts:

Dinter, D., 1989, Flexural behavior of the central Ionian Sea lithosphere due to subduction at the Hellenic trench: Constraints imposed by gravity data, preliminary manuscript.

PhD theses:

Kruse, S., 1989, Flexure of the Adriatic lithosphere (Italy) through time, Chapter 2 in "Deformation of continental lithosphere: Studies in the Ural mountains, the Adriatic region, and the western United States, PhD thesis (MIT), p. 42-149.

Figure 1.

Figure 2.

Figure 3a. Location map for the thrust belt systems examined in this study. Thrust belts associated with back-arc extension (Apennines, Carpathians and Hellenides) are indicated with lighter lines and open barbs. Thrust belts without back-arc extension (Alps and Himalaya) are indicated with darker lines and solid barbs. Regions of back-arc extension are also shown.

Figure 3b. Location map for the thrust belt systems examined in this study. Thrust belts associated with back-arc extension (Apennines, Carpathians and Hellenides) are indicated with lighter lines and open barbs. Thrust belts without back-arc extension (Alps and Himalaya) are indicated with darker lines and solid barbs. Regions of back-arc extension are also shown.

Figure 4. Profile through the Apennines for an assumed elastic plate thickness of 30 km, showing:

top) observed Bouguer gravity (dots), computed Bouguer gravity for best-fit flexural model (continuous line), and computed anomalies if Airy compensated (dashed line);

middle) initial water depth of foreland computed during flexural fitting (dashed line) and observed topography and bathymetry (continuous line);

bottom) observed depth of basin (dots); computed depth of basin for best-fit flexural model (continuous line); and computed deflection if topographic loads are not incleded in the load (only subduction forces act on the subducted plate at depth). Topography and bathymetry are also shown.

Figure 5. Profile through the Himalayas for an assumed elastic plate thickness of 90 km, showing:

top) observed Bouguer gravity (dots), computed Bouguer gravity for best-fit flexural model (continuous line), and computed anomalies if Airy compensated (dashed line);

middle) initial water depth of foreland computed during flexural fitting (dashed line) and observed topography and bathymetry (continuous line);

bottom) observed depth of basin (dots); computed depth of basin for best-fit flexural model (continuous line); and computed deflection if topographic loads are not incleded in the load (only subduction forces act on the subducted plate at depth). Topography and bathymetry are also shown.

Figure 6. Illustration of three sources of load that may act on subducted slab to produce flexural bending. (1) Topographic or surface load is equal to weight of all material present above initial depth, $w_O$, of surface of slab prior to flexure; (2) subsurface or hidden load corresponds to any other loads applied to subducted slab at depth and not expressed in surface topography; (3) infilling material, nappes, sediments, etc., present below initial slab depth $w_O$ and above final position of slab surface $w$, amplifies effects of loads 1 and 2, and can be calculated from loads 1 and 2 and flexural properties of subducted lithosphere.

Figure 7. Idealized sketch showing the relative contributions to total deflection (continuous line) from the topographic load (short dashes) and from the shear forces and bending moments acting on the plate end (long dashes). For the Apennine analog the mountains above the deflected plate were taken to have an average elevation of 1 km across a width of 40 km. For the Himalayan analog the mountains above the deflected plate were taken to have an average elevation of 5 km across a width of 500 km. In both cases the vertical shear force acting on the plate end was taken to be $4 \cdot 10^{12}$ N/m (downward) and the bending moment was taken to be $2 \cdot 10^{17}$ N (downward). Note that in the Apennine analog most of the deflection is due to the terminal shear force and bending moment, in the Himalayan analog all of the deflection in front of the mountains is due to the topographic load.

Figure 8a. Stratigraphic cross-section from the Himalayan foredeep showing the continuous forelandward migration of formations. Approximate ages for formations are: Upper Siwaliks - Pliocene-Quaternary; Middle Siwaliks - Late Miocene; Lower Siwaliks - Middle Miocene; Dharamsala - Oligocene to Early Miocene. From Lyon-Caen and Molnar (1985).

Figure 8a. Stratigraphic cross-section from the Early Proterozoic Kilohigok basin showing that the outer flexural bulge remains fixed (over the Gordon Bay arch) throughout basin evolution - note repeated erosional unconformities in this area. The basal unit (Kimerot Platform) is a shallow marine sequence, so that the basin stratigraphy is not controlled by initial, preflexural water depths. From Grotzinger and McCormick (1988).

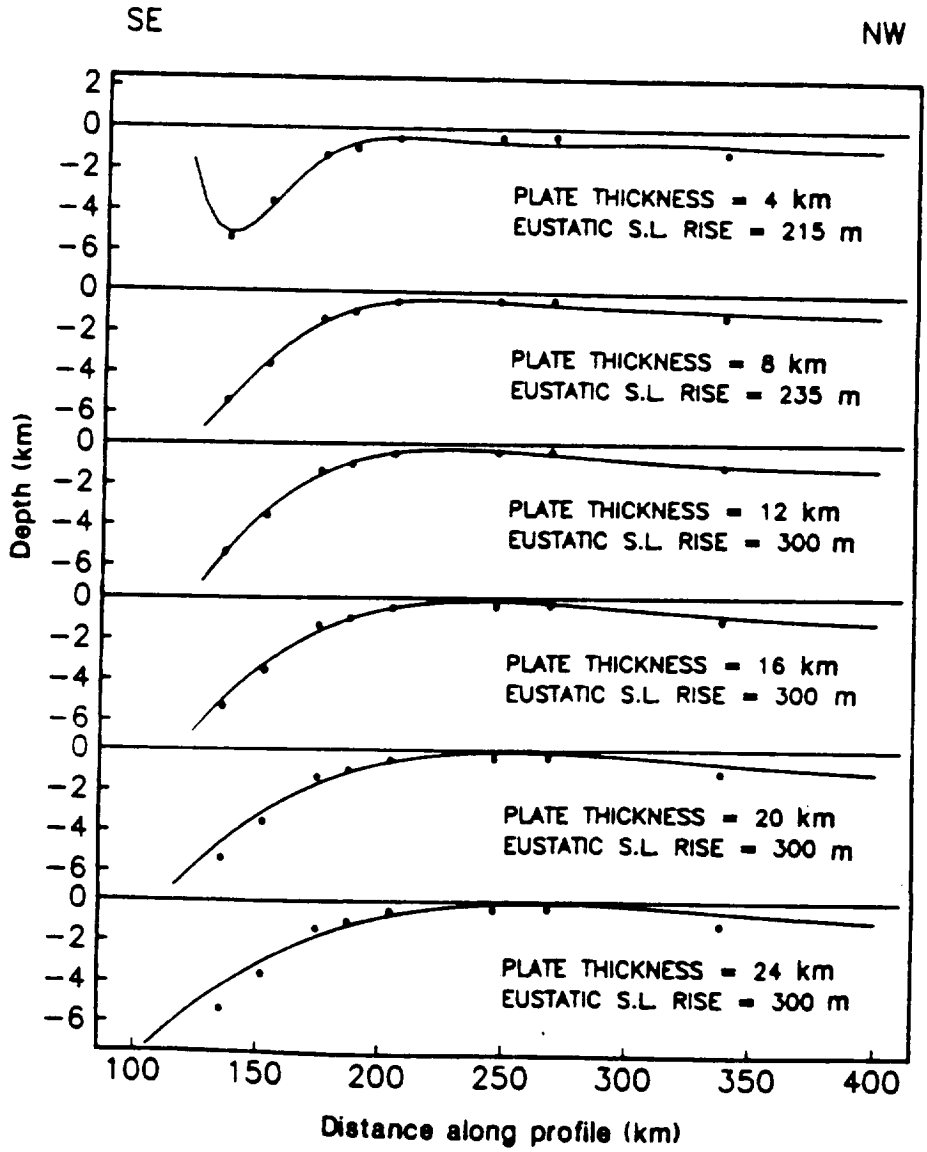


Figure 1. Depth of the Kilohigok basin determined from statigraphic sections at locations 1–8 in Fig. 1 and corrected for compaction (dots), and best-fitting theoretical flexural profiles for effective elastic plate thicknesses from 4 to 24 km (lines). Deposition at top and base of the section was constrained to have occurred at sea level, with a eustatic sea level rise of no more than 300 m.

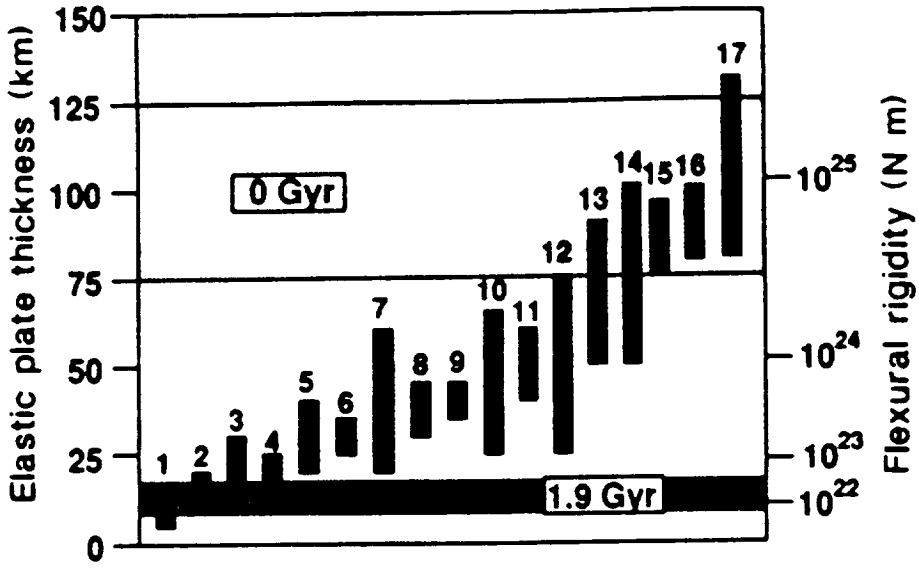


Figure 2. Comparison of flexural rigidity (shaded) of the Slave craton at 1.9 Gyr (this paper) and for the Canadian shield at present[24]. Vertical bars show reliable estimates of flexural rigidity for Phanerozoic foreland basins and convergent zones located within continental crust: 1, Transverse Ranges[25]; 2, Pamirs[26]; 3, Apennines[12]; 4, Taiwan (D. McCormick, unpublished data); 5, Carpathians[27]; 6, Alps (ref. 28 and L. Royden, unpublished data); 7, Tien Shan[29]; 8, East Texas (Ye Hungzhuan, unpublished data); 9, Kunlun[30]; 10, Andes[31]; 11, Verkoyansk[29]; 12, Zagros[32]; 13, Hellenic trench (D. Dinter, unpublished data); 14, Urals[26,33]; 15, Caucusus[34]; 16, Himalayas[35]; 17, Appalachians[28].

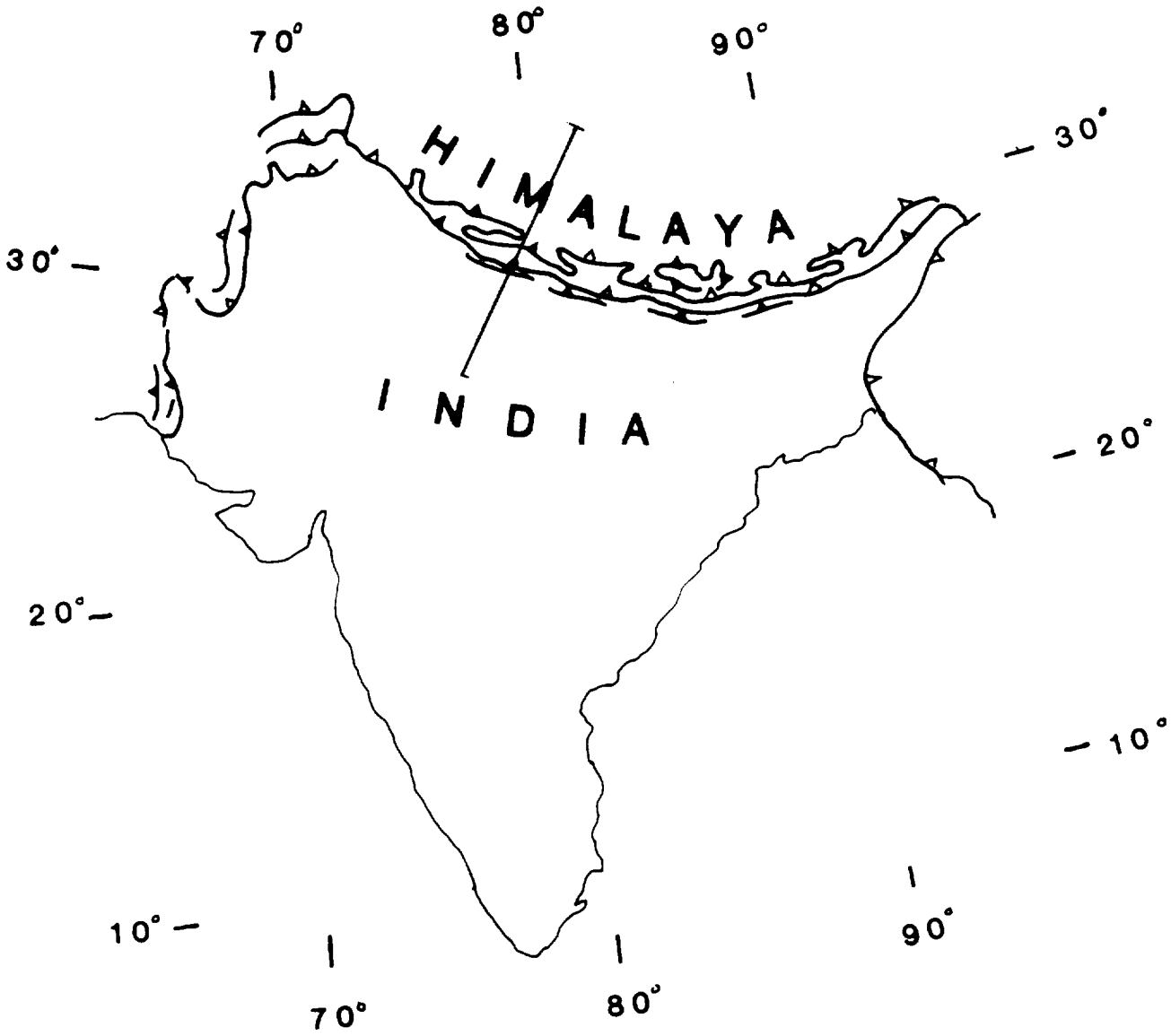


Figure 3a.

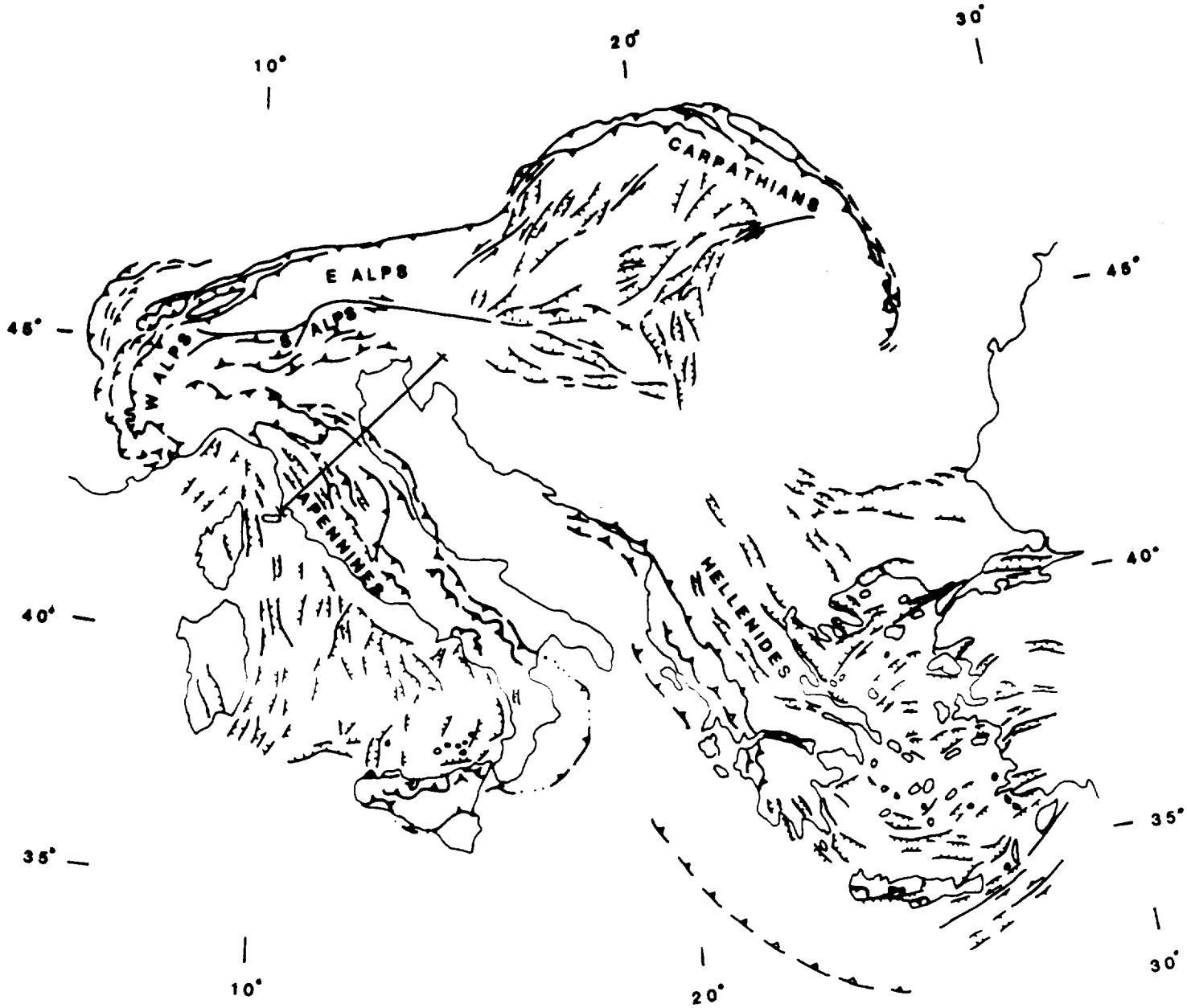


Figure 3b.

Figure 3. Location maps (Figures 3a and 3b) for the thrust belt systems examined in this study. Thrust belts associated with back-arc extension (Apennines, Carpathians and Hellenides) are indicated with lighter lines and open barbs. Thrust belts without back-arc extension (Alps and Himalaya) are indicated with darker lines and solid barbs. Regions of back-arc extension are also shown.

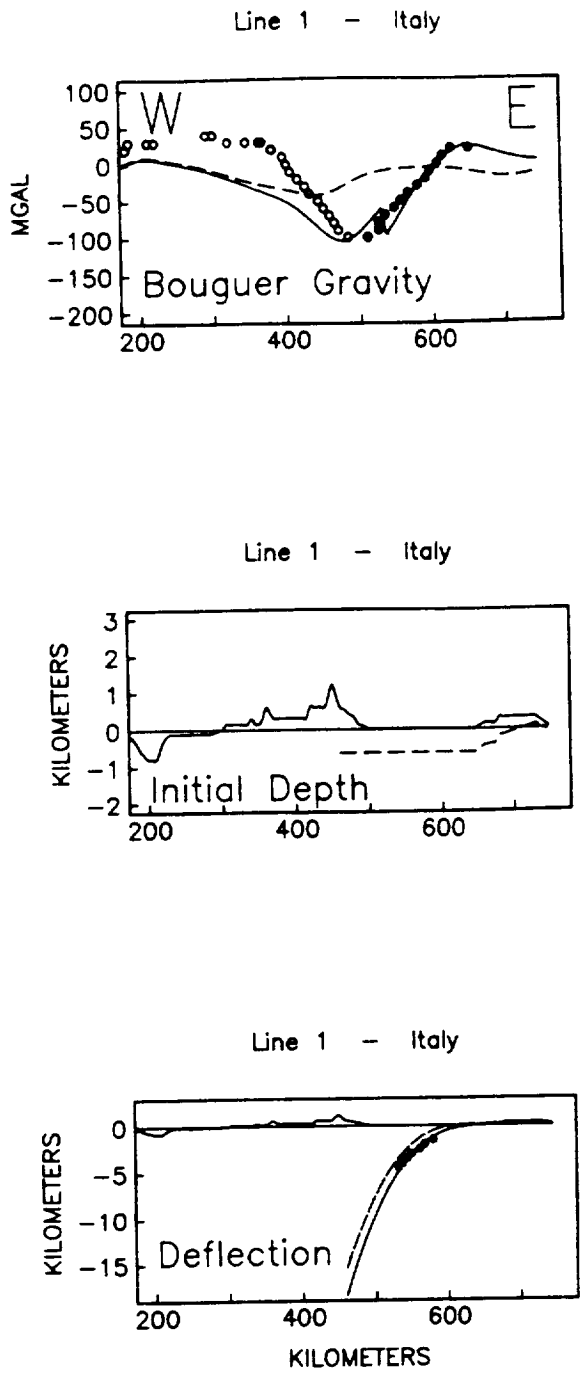


Figure 4. Profile through the Apennines for an assumed elastic plate thickness of 30 km, showing:

top) observed Bouguer gravity (dots), computed Bouguer gravity for best-fit flexural model (continuous line), and computed anomalies if Airy compensated (dashed line);

middle) initial water depth of foreland computed during flexural fitting (dashed line) and observed topography and bathymetry (continuous line);

bottom) observed depth of basin (dots); computed depth of basin for best-fit flexural model (continuous line); and computed deflection if topographic loads are not incleded in the load (only subduction forces act on the subducted plate at depth). Topography and bathymetry are also shown.

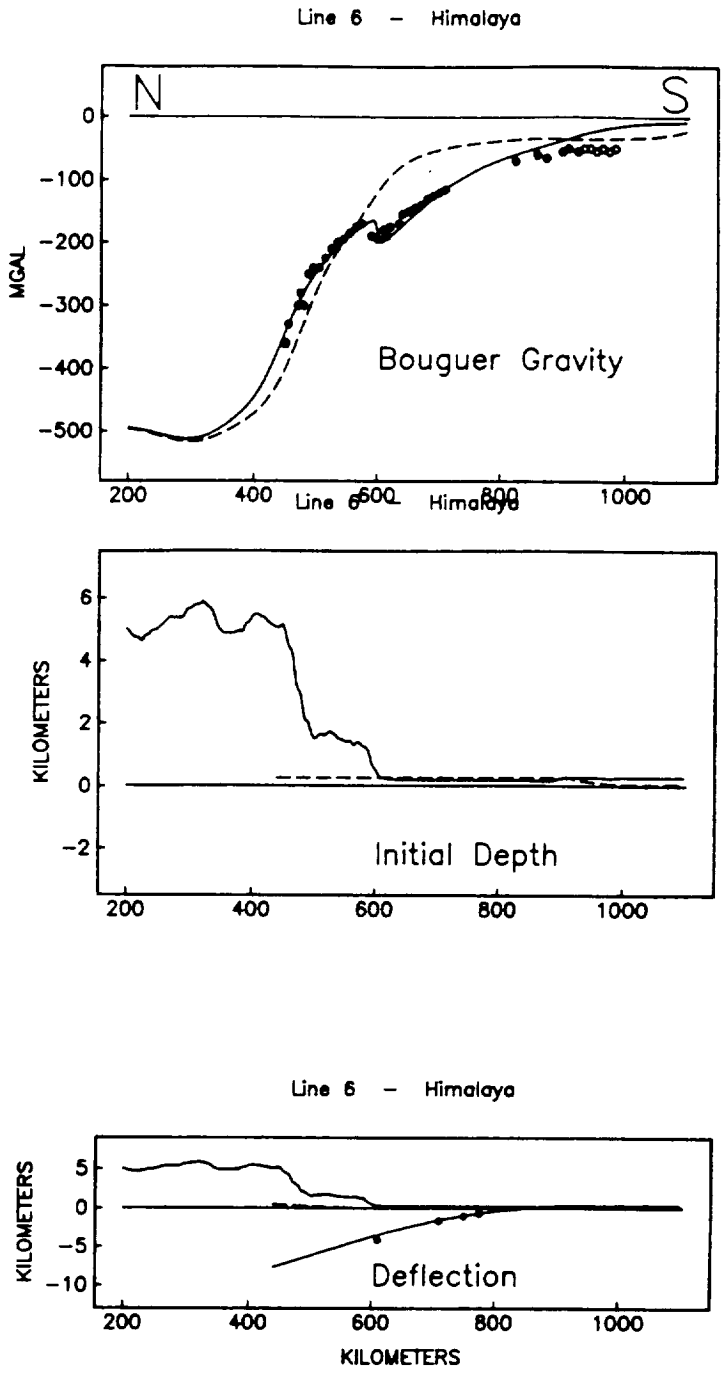


Figure 5. Profile through the Himalayas for an assumed elastic plate thickness of 90 km, showing:

top) observed Bouguer gravity (dots), computed Bouguer gravity for best-fit flexural model (continuous line), and computed anomalies if Airy compensated (dashed line);

middle) initial water depth of foreland computed during flexural fitting (dashed line) and observed topography and bathymetry (continuous line);

bottom) observed depth of basin (dots); computed depth of basin for best-fit flexural model (continuous line); and computed deflection if topographic loads are not incleded in the load (only subduction forces act on the subducted plate at depth). Topography and bathymetry are also shown.

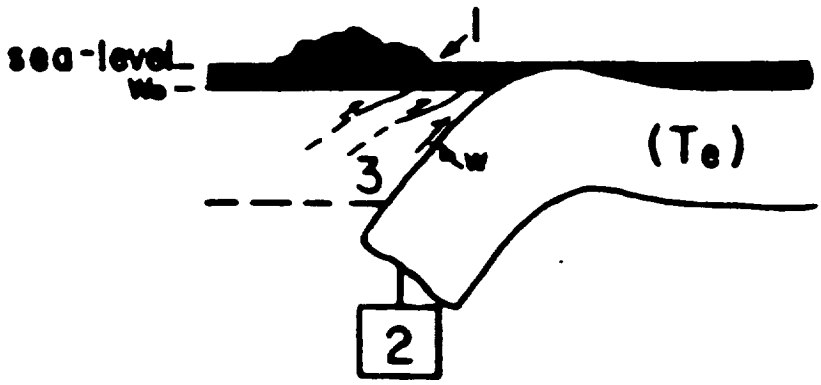


Figure 6. Illustration of three sources of load that may act on subducted slab to produce flexural bending. (1) Topographic or surface load is equal to weight of all material present above initial depth, $w_O$, of surface of slab prior to flexure; (2) subsurface or hidden load corresponds to any other loads applied to subducted slab at depth and not expressed in surface topography; (3) infilling material, nappes, sediments, etc., present below initial slab depth $w_O$ and above final position of slab surface $w$, amplifies effects of loads 1 and 2, and can be calculated from loads 1 and 2 and flexural properties of subducted lithosphere.

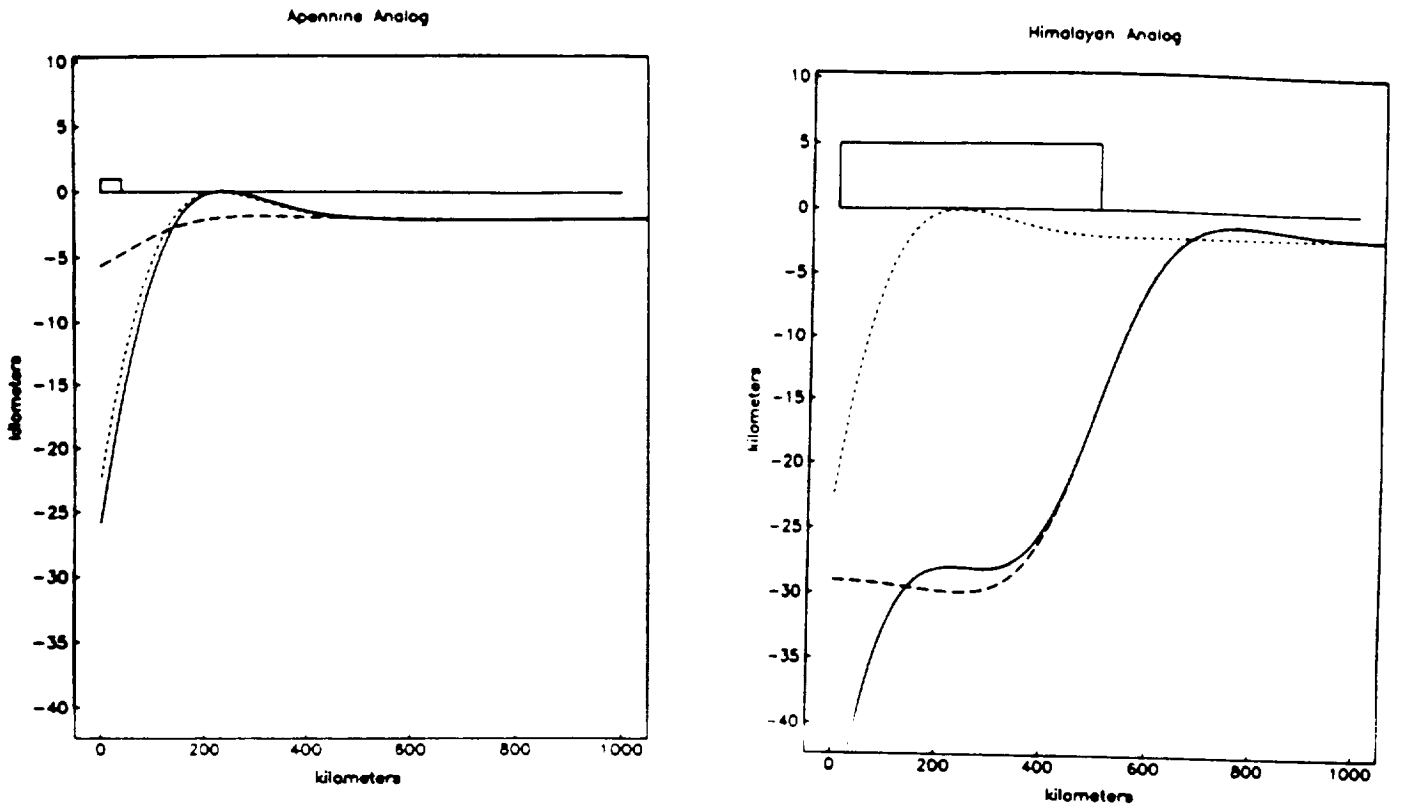


Figure 7. Idealized sketch showing the relative contributions to total deflection (continuous line) from the topographic load (short dashes) and from the shear forces and bending moments acting on the plate end (long dashes). For the Apennine analog the mountains above the deflected plate were taken to have an average elevation of 1 km across a width of 40 km. For the Himalayan analog the mountains above the deflected plate were taken to have an average elevation of 5 km across a width of 500 km. In both cases the vertical shear force acting on the plate end was taken to be $4 \cdot 10^{12}$ N/m (downward) and the bending moment was taken to be $2 \cdot 10^{17}$ N (downward). Note that in the Apennine analog most of the deflection is due to the terminal shear force and bending moment, in the Himalayan analog all of the deflection in front of the mountains is due to the topographic load.

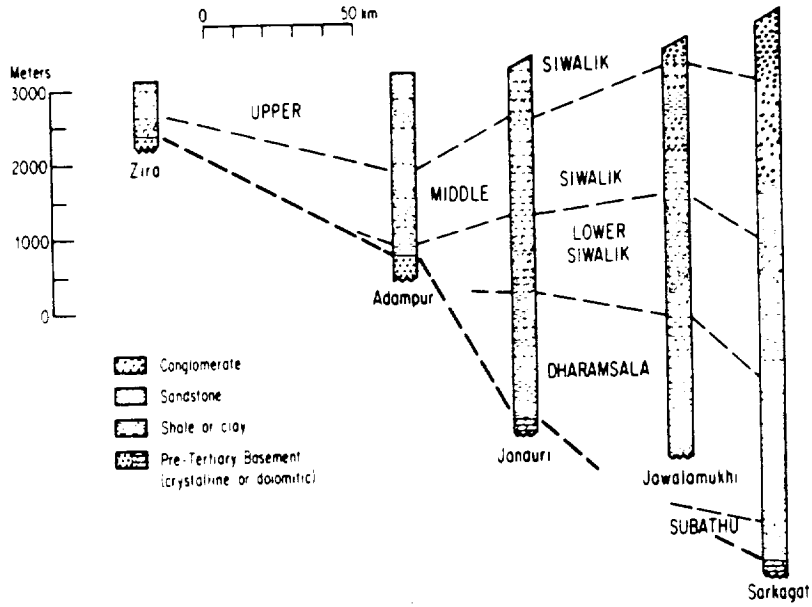


Figure 8a. Stratigraphic cross-section from the Himalayan foredeep showing the continuous forelandward migration of formations. Approximate ages for formations are: Upper Siwaliks - Pliocene-Quaternary; Middle Siwaliks - Late Miocene; Lower Siwaliks - Middle Miocene; Dharamsala - Oligocene to Early Miocene. From Lyon-Caen and Molnar (1985).

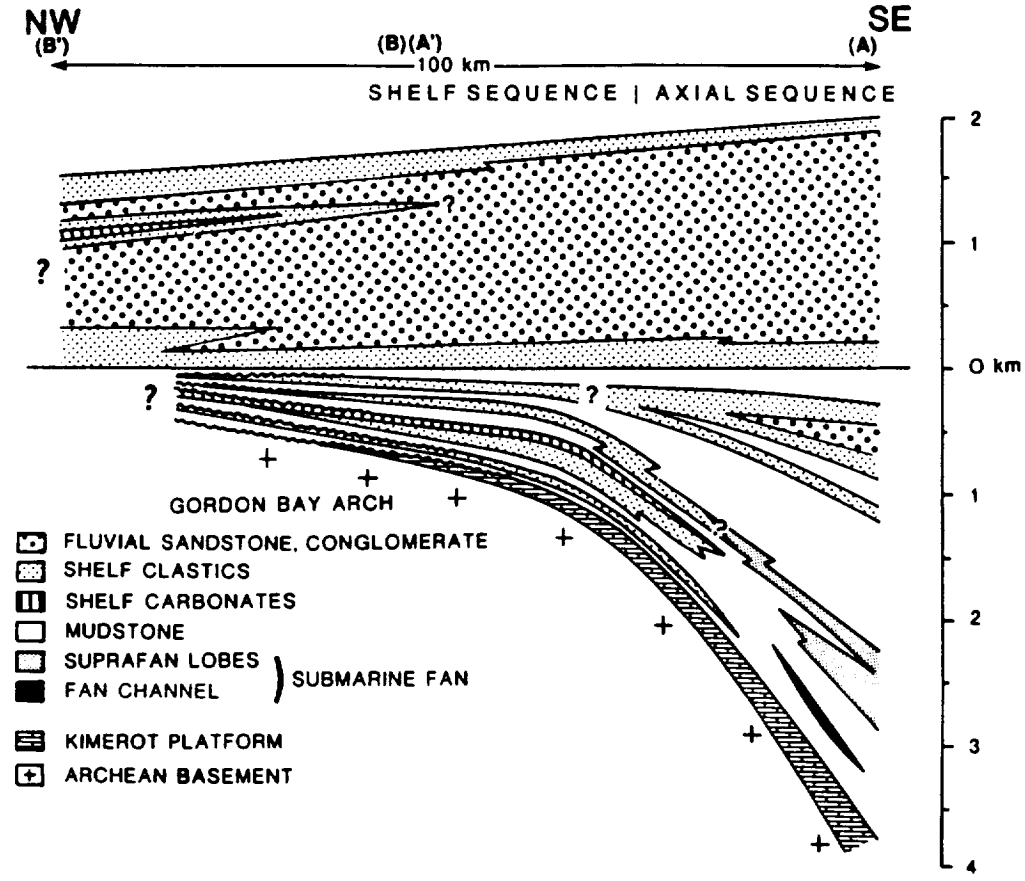


Figure 8b. Stratigraphic cross-section from the Early Proterozoic Kilohigok basin showing that the outer flexural bulge remains fixed (over the Gordon Bay arch) throughout basin evolution - note repeated erosional unconformities in this area. The basal unit (Kimerot Platform) is a shallow marine sequence, so that the basin stratigraphy is not controlled by initial, preflexural water depths. From Grotzinger and McCormick (1988).